Hybrid Monopulse-Deep-Learning-Based Blind-Spot Compensation for Full-Azimuthal Leaky-Wave Antenna Systems

Alejandro Gil-Martínez, Jesus Perez-Valero, Julien Sarrazin, *Senior Member, IEEE*, Guido Valerio, *Senior Member, IEEE*, José Luis Gómez-Tornero, *Senior Member, IEEE* and Antonio Skarmeta, *Senior Member, IEEE*

***Abstract*—This work presents a full-azimuth localization framework for ISAC based on a triangular array of bi-directional leaky-wave antennas (LWAs) and a hybrid monopulse deep-learning algorithm. Although multi-antenna arrays enable full coverage, they inherently exhibit angular blind spots where directive radiation is absent, degrading monopulse-based estimation. To address this, a lightweight neural network is combined with classical amplitude monopulse to correct systematic errors, particularly in blind-spot regions and low-SNR conditions. Using measured radiation data from a three-element LWA array, three approaches are evaluated: monopulse-only, deep-learning-only, and the proposed hybrid method. Results show that the hybrid approach significantly reduces angular error in blind spots while preserving the interpretability and low complexity of monopulse estimation. This demonstrates that AI-assisted processing enhances angular robustness in LWA-based ISAC systems without requiring hardware modifications.**

***Index Terms*—Leaky-wave antenna, direction finding, deep learning, integrated sensing and communication**

I. Introduction

MODERN communication systems, such as 5G NR and future 6G, aim to provide personalized services through accurate localization integrated into communication infrastructures [1]. This paradigm, known as integrated sensing and communication (ISAC), combines radar and communication functionalities to enhance network performance [2], [3]. In this context, direction finding (DF) is a key task in sensing systems, directly impacting localization, tracking, and beamforming [4].

Leaky-wave antennas (LWAs) are attractive due to their passive beam-scanning capability and compactness, enabling wide angular coverage without complex feeding networks [5], [6]. However, single-element LWAs exhibit limited angular responses [7]- [8], leading to reduced field-of-view (FoV) in line-of-sight (LOS) and preventing localization in non-line-of-sight (NLOS) regions [7]. This limitation is critical in full-azimuth applications. To address it, several 360° DF solutions have been proposed, using an antenna rotator [9], [10], circular arrays [11], switched beams [12], [13], and parasitic arrays [14]. Nevertheless, adjacent beams may not overlap at their half-power beamwidth (HPBW), creating angular discontinuities or shadow regions with low received power (Fig. 1). This degrades the accuracy of DF algorithms such as monopulse, MUSIC, Fingerprinting, or ESPRIT [7], [15]- [16].

Recent advances in machine learning (ML) and deep learning (DL) for ISAC [17] have shown strong performance in inverse electromagnetic problems, including pattern synthesis,

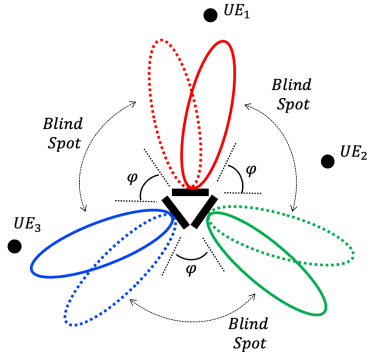

Fig. 1: Hybrid LOS/NLOS communication and sensing scenario.

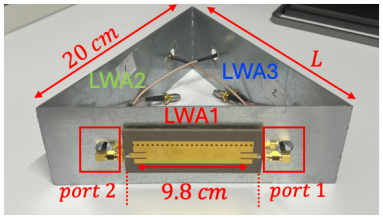

Fig. 2: Manufactured 3-LWA array.

direction-of-arrival (DoA) estimation, and ambiguity mitigation [18], [19]. In parallel, NLOS mitigation has been widely studied. Classical approaches, such as Kalman and particle filters, exploit prediction and statistical modeling to reduce NLOS errors [20], [21]. Hybrid strategies combining complementary observables (e.g., TDoA with DoA [22], AoD with RTT [23], or ToA with DoA [24]) further improve robustness. More recently, data-driven methods have demonstrated strong capabilities for NLOS detection and compensation in multipath scenarios [25]– [26]. This work proposes three techniques to enhance direction-finding accuracy in full-azimuth LWA arrays and mitigate angular shadow regions: (i) an amplitude-monopulse method based on six-port measurements; (ii) a CNN that directly estimates DoA from power snapshots; and (iii) a hybrid Monopulse-CNN approach that refines a coarse monopulse estimate via residual learning. Regarding the CNN architecture of the third approach, it is inspired by prior works [27], [28], and therefore the main novelty lies in learning only the monopulse residual error, differentiating it from purely data-driven [29] and classical monopulse methods [30]. Finally, all methods are validated using measured patterns from a three-element LWA array, focusing on error reduction in blind-spot regions under different SNR conditions.

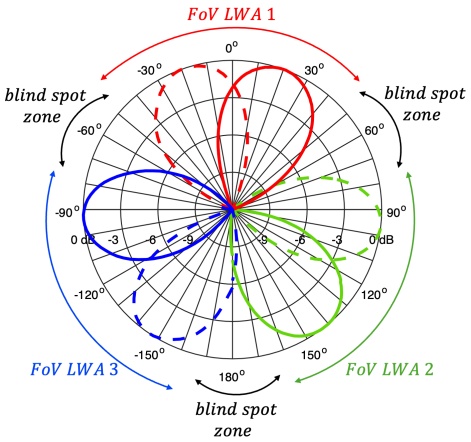

Fig. 3: Normalized full-azimuthal measured radiation patterns of the three LWA array. Solid line: port 1 of each LWA. Dotted line: port 2 of each LWA in the array.

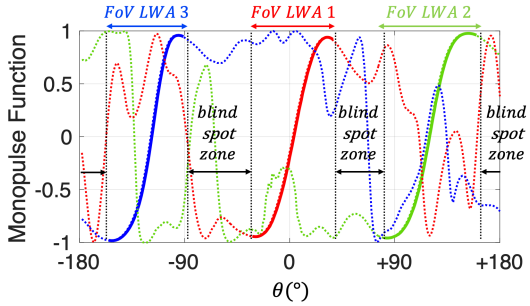

Fig. 4: Computed monopulse functions.

II. Full-Azimuth LWA Array

The proposed full-azimuth direction-finding array is based on three identical microstrip leaky-wave antennas (MLWAs) arranged in an equilateral triangular configuration to provide continuous 360° coverage, as shown in Fig. 2. Each MLWA corresponds to the compact bidirectionally fed design reported in [31], operating at $f_0 = 2.402$ GHz. The total electrical length of a single antenna is approximately $L \approx 0.8\lambda_0$ ($L = 98$ mm), producing two directive beams when excited from opposite ports at $\varphi_R = \pm 15°$, each with a half-power beamwidth (HPBW) of approximately 60°.

Three identical MLWAs are positioned on a circular ground plane forming an equilateral triangle, with their main radiation axes oriented at

$$\theta_n = \theta_0 + n \cdot 120°, \quad n = 0, 1, 2. \tag{1}$$

The array has been calibrated and measured in an anechoic chamber using a multi-port VNA. The resulting full-azimuth radiation patterns at $f_0 = 2.39$ GHz are depicted in Fig. 3. All six ports exhibit consistent performance, with $S_{11} < -10$ dB in 2.4–2.6 GHz, peak gain of 1.59–1.7 dB, radiation efficiency of 55%–59%, and HPBW of 43°–48°. These small variations, mainly due to fabrication tolerances affecting antenna width (beam direction) and length (HPBW), do not compromise the distinct angular coverage required for the sensing application.

A. System Model

Let $\theta \in [-180°, 180°]$ denote the DoA of a single far-field source. The measured radiation patterns of the six available ports (three antennas, two ports each) are used to define the array response in terms of received power. Specifically, let

$$\mathbf{g}(\theta) = \begin{bmatrix} g_1(\theta) & g_2(\theta) & \cdots & g_6(\theta) \end{bmatrix}^T \tag{2}$$

be the vector of calibrated radiation patterns obtained from anechoic chamber measurements, sampled over the full azimuth plane with 1° resolution.

Assuming a single source with average transmitted power P_s, the received signal at the m-th port for the k-th snapshot is modeled as

$$P_m[k] = P_s\, g_m(\theta) + w_m[k], \tag{3}$$

where $P_m[k]$ denotes the measured received power and $w_m[k] \sim \mathcal{N}(0, \sigma^2)$ accounts for additive Gaussian noise.

Stacking the six ports, the observation vector is given by

$$\mathbf{p}[k] = P_s\, \mathbf{g}(\theta) + \mathbf{w}[k], \quad k = 1, \ldots, K, \tag{4}$$

where $K = 1000$ snapshots are considered in this work, as the estimation performance stabilizes for K above 500 snapshots.

Based on the measured patterns in Fig. 3, certain angular regions exhibit low received power across all ports. These regions, referred to as angular shadow regions, can be formally defined as

$$\mathcal{S} = \{\theta \mid \|\mathbf{g}(\theta)\|_2 < \epsilon\}, \tag{5}$$

where ϵ is a threshold related to the system sensitivity.

III. Direction-Finding Strategies Under LOS/NLOS Conditions

This section describes the three direction-finding strategies evaluated in this work to mitigate the angular degradation caused by shadow regions in the full-azimuth LWA array. The methods are: a classical amplitude-monopulse technique, a purely data-driven deep learning approach, and a hybrid model that combines physical monopulse features with learning-based correction.

A. Monopulse-Only Direction Finding

For a signal impinging from an angle θ_0, the received power vector across the six ports is modeled, according to the system model, as

$$\mathbf{p}[k] = P_s\, \mathbf{g}(\theta_0) + \mathbf{w}[k], \tag{6}$$

where $\mathbf{g}(\theta)$ is the array response vector in power and $\mathbf{w}[k]$ represents additive noise.

For a single MLWA, the conventional monopulse function is:

$$\mathrm{MF}(\theta) = \frac{\Delta(\theta)}{\Sigma(\theta)}, \tag{7}$$

with $\Sigma(\theta)$ and $\Delta(\theta)$ being the sum and difference radiation patterns (in power) of two consecutive beams, respectively. $\mathrm{MF}(\theta)$ is approximately linear near the perpendicular direction between the beams that form the monopulse pattern, i.e.,

$$\mathrm{MF}(\theta) \approx K \cdot (\theta - \theta_p), \tag{8}$$

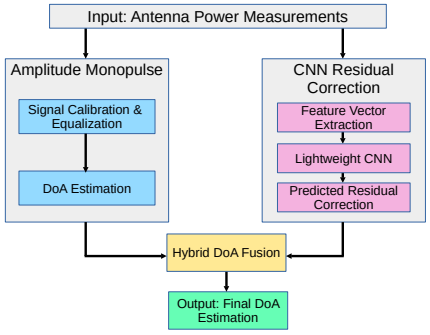

Fig. 5: Conceptual diagram of the proposed hybrid Monopulse-CNN DoA estimation model.

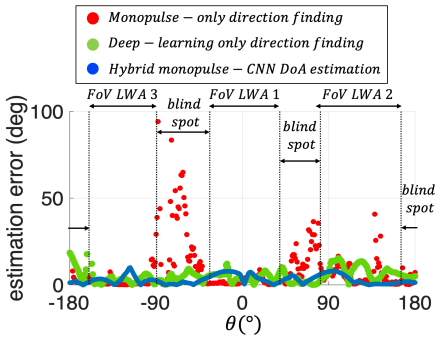

Fig. 6: Absolute angular error of the proposed algorithms over the full azimuth range.

where K is the monopulse slope and θ_p the perpendicular angle. The computed monopulse functions from measured radiation patterns are shown in Fig. 4. As commented, three MFs with linear slopes are obtained for each beam pattern combination in the LWA array. However, near the sector boundaries where $\Sigma(\theta)$ decreases due to low overlap, the linearity of MF(θ) breaks down, yielding blind-spot zones with large angular errors [7].

This motivates the application of deep learning estimators to reconstruct accurate θ_0 values across the entire azimuth range without adding extra hardware complexity to the antenna design.

B. Deep-Learning-Only Direction Finding

To overcome the limitations of classical amplitude-monopulse estimation in blind-spot regions, a purely data-driven direction-finding approach is investigated. The DoA estimation problem is formulated as a nonlinear regression task, where a lightweight convolutional neural network (CNN) directly maps the measured electromagnetic responses of the LWA array to the corresponding azimuth angle.

Let $\mathbf{x} \in \mathbb{R}^{M\times K}$ denote the input data matrix. The input tensor is constructed by stacking the normalized power samples of all channels. The CNN implements a parametric nonlinear mapping

$$\hat{\boldsymbol{y}} = f_{\boldsymbol{\theta}}(\mathbf{x}), \tag{9}$$

where $f_{\boldsymbol{\phi}}(\cdot)$ denotes the CNN with trainable parameters $\boldsymbol{\phi}$. The network consists of a single one-dimensional convolutional layer operating along the snapshot dimension, followed by a rectified linear unit (ReLU) activation and a global average pooling stage. The convolution operation is given by

$$\mathbf{h} = \sigma(\mathbf{W} * \mathbf{x} + \mathbf{b}), \tag{10}$$

where $\mathbf{W}$ denotes the convolution kernels, $\mathbf{b}$ the bias vector, and $\sigma(\cdot)$ the ReLU activation function.

Instead of directly regressing the azimuth angle, the network output is a two-dimensional vector

$$\hat{\boldsymbol{y}} = [\hat{y}_1, \hat{y}_2] = \begin{bmatrix} \sin(\hat{\theta}_0) \\ \cos(\hat{\theta}_0) \end{bmatrix}, \tag{11}$$

which ensures angular continuity and avoids discontinuities at $\pm 180°$. The final DoA estimate is recovered as

$$\hat{\theta}_0 = \arg(\hat{y}_2 + j\,\hat{y}_1), \tag{12}$$

The CNN is trained in a supervised manner by minimizing the mean squared error between the predicted and ground-truth sine–cosine representations:

$$\mathcal{L}(\boldsymbol{\phi}) = \frac{1}{N}\sum_{i=1}^{N} \|\hat{\boldsymbol{y}}_i - \boldsymbol{y}_i\|_2^2, \tag{13}$$

where N denotes the total number of training samples, and $\boldsymbol{y}_i = [\sin(\theta_{0,i}), \cos(\theta_{0,i})]^\top$.

C. Hybrid Monopulse–CNN Direction Finding

Here, we propose a hybrid approach (depicted in Fig. 5) combining the robustness and physical interpretability of classical monopulse processing (left branch) with the representational power of CNNs (right branch). Instead of directly learning the azimuth angle, the CNN is trained to predict the residual error of the monopulse estimator.

Regarding the training procedure, the CNN architecture consists of a single one-dimensional convolutional layer with $K = 8$ filters and a temporal kernel size of $L = 15$, followed by ReLU activation and global average pooling, culminating in a scalar output that directly estimates the residual angular correction $\Delta\theta_{\text{CNN}}$. Training is performed using full-batch gradient descent with a learning rate of 1×10^{-4} over 20 epochs. The hybrid direction-finding algorithm operates as shown in Algorithm 1.

IV. Performance Evaluation

The performance of the proposed direction-finding algorithms is evaluated over the full azimuth range from $-180°$ to $180°$. For each azimuth angle, $k = 1000$ simulated snapshots are generated with a constant SNR of 20 dB (resulting in a total of 361,000 samples), allowing a statistically meaningful assessment of the estimation error. For the CNN-only and hybrid models, the dataset was split into 80% for training, 10% for validation, and 10% for testing. Additionally, independent noise realizations are used for each snapshot during both training and evaluation.

In terms of the training platform, all models were implemented in MATLAB R2023b and trained on a standard workstation equipped with an Intel Core i7-12700K CPU @ 3.60 GHz, 32 GB of RAM. Training loss curves demonstrate convergence within 50 epochs for the CNN-only model and below 20 epochs for the hybrid algorithm.

The absolute error for each algorithm across the full 360° field of view (FoV) is illustrated in Fig. 6, while the overall

Algorithm 1 Hybrid Monopulse–CNN DoA Estimation

1) Acquire the received power snapshots from the full-azimuth LWA array $\mathbf{p}[k]$.
2) Compute the monopulse values associated with the received instant power from each beam pair and a certain angle θ_0:
$$\mathrm{MV}_{i,j} = \frac{P_i - P_j}{P_i + P_j} \tag{14}$$
where (i, j) are the indices of a given monopulse pair.
3) Generate the angular pseudospectrum for each monopulse function:
$$\mathrm{APS}_n(\theta) = -10\log_{10}\left(\frac{1}{|\mathrm{MF}_n(\theta) - \mathrm{MV}_n|}\right) \tag{15}$$
where the index $n = 1, \ldots, N$ enumerates the N monopulse combinations.
4) Fuse all pseudospectra into a global angular response:
$$\mathrm{APS}_{\mathrm{MP}}(\theta) = \mathcal{F}\{\mathrm{APS}_1(\theta), \ldots, \mathrm{APS}_N(\theta)\} \tag{16}$$
5) Estimate the preliminary DoA from the maximum of the fused pseudospectrum:
$$\hat{\theta}_{\mathrm{MP}} = \arg\max_{\theta}\{\mathrm{APS}_{\mathrm{MP}}(\theta)\} \tag{17}$$
6) Construct the feature vector using monopulse values and RSS measurements:
$$\mathbf{x} = \left[\mathrm{MV}_1, \ldots, \mathrm{MV}_N,\ P_1, \ldots, P_M,\ \hat{\theta}_{\mathrm{MP}}\right]^\top \tag{18}$$
7) Feed the feature vector into the trained CNN:
$$\Delta\theta_{\mathrm{CNN}} = f_{\boldsymbol{\theta}}(\mathbf{x}) \tag{19}$$
8) Compute the final DoA estimate:
$$\hat{\theta} = \hat{\theta}_{\mathrm{MP}} + \Delta\theta_{\mathrm{CNN}} \tag{20}$$

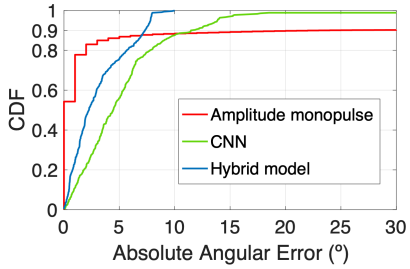

Fig. 7: Cumulative Distribution Function (CDF) of the proposed algorithms.

	RMSE (deg)			MAE (deg)		
SNR	10	20	40	10	20	40
Monopulse-only	88.6	36.4	12.8	60	8.1	1.1
CNN-only	38.7	33.9	5	9.6	8.5	1.3
Hybrid Monopulse-CNN	4.7	3.9	2.7	3.2	2.8	0.9

TABLE I: DoA Estimation Error for the proposed algorithms. root mean square error (RMSE) and mean absolute error (MAE) values are summarized in Table I.

From Fig. 6, the monopulse-only algorithm exhibits large angular errors in shadow regions where the received power is below sensitivity, while performing accurately in LOS regions. This behavior is reflected by the red dots in Fig. 6. The CNN-only model (green dots in Fig. 6) estimates the location across all azimuth angles, capturing nonlinear distortions and compensating for blind-spot zones. Nevertheless, Table I reports RMSE/MAE for SNR = 10, 20, 40 dB, where the hybrid method consistently outperforms the others, especially at low SNR. At SNR = 20 dB, separate LOS/blind-spot analysis shows that the hybrid approach maintains high accuracy in both regions (RMSE 4.4° and 3.9°, respectively), whereas monopulse-only degrades severely in blind spots (RMSE 55.2°). However, CNN-only does not fully exploit the physical structure of the problem. The hybrid monopulse–CNN algorithm (blue dots in Fig. 6) combines the interpretability and coarse accuracy of the monopulse estimator with CNN-based residual correction, removing shadow-region failures and reducing error across the entire FoV.

Fig. 7 shows the cumulative distribution function (CDF) of the absolute angular error for the three algorithms over the full 360° FoV. The amplitude-monopulse method exhibits a slow-rising CDF with a heavy tail, indicating a high probability of large errors, mainly due to shadow regions where the monopulse ratio becomes unreliable. The CNN-only approach improves the distribution, reducing outliers and producing a steeper CDF, although its performance is limited by a residual error floor, yielding accuracy comparable to monopulse (Table I). In contrast, the proposed Monopulse-CNN method achieves a significantly steeper CDF, concentrating most probability at low errors. This confirms its ability to mitigate blind-spot failures and enhance accuracy across the entire FoV.

D. Operating Efficiency Comparison

We extended our performance evaluation to include a comparison of the three methods in terms of operation efficiencies. We find that the Monopulse-only method is the fastest (0.027 ms per angle) and has the fewest operations ($\sim 3.6 \times 10^2$ FLOPs per angle) due to its simple arithmetic operations. The CNN-only method is the slowest (0.371 ms per angle, $\sim$14$\times$ slower than baseline) and most computationally intensive ($\sim 1.3 \times 10^5$ FLOPs per angle), due to convolutions over the input tensor. The Hybrid Monopulse-CNN method offers a trade-off: inference time of 0.268 ms per angle ($\sim$1.4$\times$ faster than CNN-only) and $\sim 1.5 \times 10^3$ FLOPs per angle, which is about 87$\times$ fewer than CNN-only. The relative cost (FLOPs ratio to Monopulse-only) is $\sim$360$\times$ for CNN-only and $\sim$4$\times$ for the Hybrid method

V. Conclusion

Three approaches for DoA estimation with a full-azimuth LWA array have been analyzed. While monopulse performance follows the antenna physics but degrades in shadow regions, and the CNN reduces errors without exploiting physical models, the hybrid approach combines both by refining the monopulse estimate through residual learning. This yields significant improvements in RMSE and MAE, demonstrating that physics-informed deep learning enables accurate and robust DoA estimation suitable for real-time applications. As future work, we plan to investigate cross-antenna beam combinations to address blind-spot regions.

ACKNOWLEDGMENT

A. Gil-Martínez, J. Perez-Valero and A. Skarmeta are with the Department of Information and Communication Engineering, Universidad de Murcia, 30100, Spain. Their work is supported by SNS JU project 6G-CLOUD (Grant Agreement no. 101139073), Programa de Universalización de Infraestructuras Digitales Para la Cohesión - 6G I+D TSI-064100-2023-13, 6G-Computing Continuum Network Infrastructure 6G-CoCoNet and TSI-064100-2022-2, Gaia 6G. Julien Sarrazin and Guido Valerio are with the Laboratoire de Génie Electrique et Electronique de Paris, CNRS, Sorbonne Université, 75252, France. Their work is supported by the ANR BeSensiCom project, grant ANR-22-CE25-0002 of the French Agence Nationale de la Recherche.

REFERENCES

[1] W. Chen, X. Lin, J. Lee, A. Toskala, S. Sun, C. F. Chiasserini, and L. Liu, "5g-advanced toward 6g: Past, present, and future," *IEEE J. Sel. Areas Commun.*, vol. 41, no. 6, pp. 1592–1619, Jun. 2023.

[2] ETSI. (2025, Mar.) Integrated sensing and communication (isac); use cases and deployment scenarios. Accessed: 2025-05-19. [Online]. Available: https://www.etsi.org/deliver/etsi_gr/ISC/001_099/001/01.01.01_60/gr_ISC001v010101p.pdf

[3] G. Kwon, A. Conti, H. Park, and M. Z. Win, "Joint communication and localization in millimeter wave networks," *IEEE J. Sel. Topics Signal Process.*, vol. 15, no. 6, pp. 1439–1454, Nov. 2021.

[4] J. A. Zhang, M. L. Rahman, K. Wu, X. Huang, Y. J. Guo, S. Chen, and J. Yuan, "An overview of signal processing techniques for joint communication and radar sensing," *IEEE J. Sel. Topics Signal Process.*, vol. 15, no. 6, pp. 1295–1315, Nov. 2021.

[5] A. A. Oliner and D. R. Jackson, "Leaky-wave antennas," in *Antenna Engineering Handbook*, 4th ed., J. L. Volakis, Ed. New York, NY, USA: McGraw-Hill, 2007.

[6] J. L. Gómez-Tornero, "Smart leaky-wave antennas for iridescent iot wireless networks," in *Antenna and Array Technologies for Future Wireless Ecosystems*, Y. J. Guo and R. W. Ziolkowski, Eds. Wiley, 2022.

[7] A. Gil-Martinez, M. Poveda-García, J. A. López-Pastor, J. C. Sánchez-Aarnoutse, and J. L. Gómez-Tornero, "Monopulse leaky wave antennas for RSSI based direction finding in wireless local area networks," *IEEE Trans. Antennas Propag.*, vol. 71, no. 11, pp. 8602–8615, 2023.

[8] M. K. Emara, E. Kupershtein, N. Grits, D. Regev, and R. Shavit, "Millimeter-wave slot array antenna front-end for amplitude-only direction finding," *IEEE Trans. Antennas Propag.*, vol. 68, no. 7, pp. 5365–5374, Jul. 2020.

[9] S. Lian, J. Wang, X. Li, Y. Zhang, and H. Chen, "Full-coverage 3-d indoor positioning system based on a rotating dual-ultra-wideband platform," *IEEE Trans. Instrum. Meas.*, vol. 74, pp. 1–10, 2025, art. no. 6502610.

[10] M. Malajner, P. Planinsic, and D. Gleich, "Angle of arrival estimation using RSSI and omnidirectional rotatable antennas," *IEEE Sensors J.*, vol. 12, no. 6, pp. 1950–1957, Jun. 2012.

[11] N. Paulino and L. M. Pessoa, "Self-localization via circular bluetooth 5.1 antenna array receiver," *IEEE Access*, vol. 11, pp. 365–395, 2023.

[12] R. Kawdungta, P. Suksompong, N. Srisamran, and K. Thongyoi, "Switched beam multi-element circular array antenna schemes for 2d single-anchor indoor positioning applications," *IEEE Access*, vol. 9, pp. 58 882–58 892, 2021.

[13] G. Giorgetti, A. Cidronali, S. K. S. Gupta, and G. Manes, "Single-anchor indoor localization using a switched-beam antenna," *IEEE Commun. Lett.*, vol. 13, no. 1, pp. 58–60, Jan. 2009.

[14] M. Rzymowski, P. Woznica, and L. Kulas, "Single-anchor indoor localization using ESPAR antenna," *IEEE Antennas Wireless Propag. Lett.*, vol. 15, pp. 1183–1186, 2016.

[15] M. Passafiume, S. Maddio, A. Cidronali, and G. Manes, "MUSIC algorithm for RSSI-based DoA estimation on standard 802.11/802.15.x systems," *WSEAS Trans. Signal Process.*, vol. 11, pp. 58–68, 2015.

[16] A. J. Weiss and M. Gavish, "Direction finding using ESPRIT with interpolated arrays," *IEEE Trans. Signal Process.*, vol. 39, no. 6, pp. 1473–1478, Jun. 1991.

[17] M. Temiz, E. Alsusa, K. A. Hamdi, A. Al-Dweik, and M. A. Imran, "Deep-learning-based techniques for integrated sensing and communication systems: State-of-the-art, challenges, and opportunities," *IEEE Open J. Commun. Soc.*, vol. 6, pp. 5940–5968, 2025.

[18] Q. Zhu, B. Ma, Y. Wang, J. Liu, and Y. Cui, "DOA estimation of multibeam frequency beam scanning LWAs based on sparse bayesian learning," *IEEE Geosci. Remote Sens. Lett.*, vol. 22, pp. 1–5, 2025.

[19] A. Gil-Martínez, J. Perez-Valero, J. A. López-Pastor, J. L. Gómez-Tornero, and A. Skarmeta-Gómez, "Ambiguity resolution of two conformal leaky-wave antennas via deep learning," in *Proc. Int. Conf. Indoor Positioning Indoor Navig. (IPIN)*, Tampere, Finland, 2025, pp. 1–7.

[20] B. Wang, B. Song, T. Wang, Z. Deng, and M. Fu, "A BDS/5G combined positioning method based on adaptive optimal selection-robust hybrid adaptive kalman filter algorithm," *IEEE Internet Things J.*, vol. 11, no. 12, pp. 22 376–22 384, Jun. 2024.

[21] N. Xia and M. A. Weitnauer, "TDOA-based mobile localization using particle filter with multiple motion and channel models," *IEEE Access*, vol. 7, pp. 21 057–21 066, 2019.

[22] S. K. Das and R. Mudi, "Kalman filter based NLOS identification and mitigation for M2M communications over cellular networks," in *Proc. IEEE Veh. Technol. Conf. (VTC-Spring)*, Helsinki, Finland, 2021.

[23] Q. Bader, S. Saleh, M. Elhabiby, and A. Noureldin, "NLoS detection for enhanced 5g mmwave-based positioning for vehicular IoT applications," in *Proc. IEEE Global Commun. Conf. (GLOBECOM)*, Rio de Janeiro, Brazil, 2022, pp. 5643–5648.

[24] A. Gaber and A. Omar, "Utilization of multiple-antenna multicarrier systems and NLOS mitigation for accurate wireless indoor positioning," *IEEE Trans. Wireless Commun.*, vol. 15, no. 10, pp. 6570–6584, Oct. 2016.

[25] A. Saeidanezhad, W. Ahmad, M. A. Imran, and O. R. Popoola, "Enhancing indoor localization accuracy in dense IoT-integrated 5gnr networks: Introducing SGNC for sensor-guided NLoS correction localization," *IEEE J. Indoor Seamless Positioning Navig.*, vol. 2, pp. 333–342, 2024.

[26] Y. Ma, L. Zhou, K. Liu, and J. Wang, "Iterative phase reconstruction and weighted localization algorithm for indoor RFID-based localization in NLOS environment," *IEEE Sensors J.*, vol. 14, no. 2, pp. 597–611, Feb. 2014.

[27] Q. Tian, R. Cai, Y. Luo, and G. Qiu, "Doa estimation: Lstm and cnn learning algorithms," *Circuits, Systems, and Signal Processing*, vol. 44, no. 1, pp. 652–669, 2025.

[28] S. Ge, K. Li, and S. N. B. M. Rum, "Deep learning approach in doa estimation: A systematic literature review," *Mobile Information Systems*, vol. 2021, no. 1, p. 6392875, 2021.

[29] A. Bohlender, A. Spriet, W. Tirry, and N. Madhu, "Exploiting temporal context in cnn based multisource doa estimation," *IEEE/ACM Transactions on Audio, Speech, and Language Processing*, vol. 29, pp. 1594–1608, 2021.

[30] A. Gil-Martinez, J. A. López-Pastor, M. Poveda-Garcia, A. Algaba-Brazález, D. Cañete-Rebenaque, and J. L. Gómez-Tornero, "Monopulse leaky wave antennas for rssi-based direction finding in wireless local area networks," *IEEE Transactions on Antennas and Propagation*, vol. 71, no. 11, pp. 8602–8615, 2023.

[31] A. Gil-Martínez, M. Poveda-García, D. Cañete-Rebenaque, A. Algaba-Brazalez, and J. L. Gómez-Tornero, "Compact amplitude-monopulse microstrip antenna design for wide field-of-view direction finding," in *Proc. Eur. Conf. Antennas Propag. (EuCAP)*, Glasgow, United Kingdom, 2024, pp. 1–5.